J. Fluid Mech. (1982), *vol.* 125, *pp.* 99–122
Printed in Great Britain

Time-dependent solutions of multimode convection equations

By JURI TOOMRE,

Joint Institute for Laboratory Astrophysics, and Department of Astrophysical, Planetary and Atmospheric Sciences, University of Colorado, Boulder, Colorado 80309, U.S.A.

D. O. GOUGH

Institute of Astronomy, and Department of Applied Mathematics and Theoretical Physics, University of Cambridge, Silver Street, Cambridge CB3 9EW, England

AND E. A. SPIEGEL

Department of Astronomy, Columbia University, New York, New York 10027, U.S.A.

(Received 31 March 1981 and in revised form 6 July 1982)

Truncated modal equations are used to study the time evolution of thermal convection. In the Boussinesq approximation these nonlinear equations are obtained by expanding the fluctuating velocity and temperature fields in a finite set of planforms of the horizontal coordinates. Here we report on numerical studies dealing with two or three modes with triad interactions. We have found rich time dependence in these cases: periodic and aperiodic solutions can be obtained, along with various steady solutions. Three-mode solutions reproduce the qualitative appearance of spoke-pattern convection as observed in experiments at high Prandtl numbers. Though the values of the periods of the time-dependent solutions do not agree with those of the experiments, their variation with Rayleigh number compares favourably. Except at the highest Rayleigh number we have considered (10^7), the theoretical Nusselt numbers agree well with experiment.

1. Introduction

In the predecessors of this paper we attempted to describe the gross features of a convecting fluid by a simple if crude approximation procedure (Gough, Spiegel & Toomre 1975*a*, hereinafter referred to as I; Toomre, Gough & Spiegel 1977, hereinafter II). We expanded the fluctuating temperature and velocity in terms of the planform functions of linear theory and kept only a few terms, or modes as we shall call them. In I and II we described calculations in which only one mode was kept, and we solved the resulting equations for the vertical structure with accurate numerical schemes. Of course, the choice of planform remains arbitrary, but nevertheless it was encouraging to learn in II that a choice exists that leads to a tolerably good representation of the mean properties of laboratory convection.

In the case of single-mode convection the solutions always evolved to steady states, which satisfy the system of equations first given by Roberts (1966). However, laboratory studies of convection become time-dependent at high enough Rayleigh number, and we would like to know whether and how well the modal approach represents this. Indeed, in two- and three-mode studies we have found sustained time dependence, both periodic and aperiodic, and we report here on these results.

Among the various solutions that we have found, perhaps the most interesting are those that describe periodic oscillations of hexagonal cells, and thus recall a qualitative behaviour found experimentally. However, from a practical point of view, we should also pay attention to the wide variety of solutions the modal procedure reveals. It is likely that the multiplicity of solutions we have found, but have not thoroughly catalogued, is indicative of a similar richness in the solution space of the full equations. The qualitative properties of modal solutions that have counterparts in experimental convection, together with the relative ease with which their equations may be solved at present, suggest that they may provide a tool for exploring the solution space of the full equations in a relatively simple way. For although it is now quite possible to solve the Boussinesq equations in three dimensions, the procedures require extensive programming and calculations. The modal equations, on the other hand, have only one space dimension and are rather easier to deal with. Hence they facilitate the study of nonlinear behaviour of the non-turbulent aspects of convection.

2. Equations

We consider a fluid in the Boussinesq approximation, of infinite horizontal extent, and bounded above and below by two horizontal plates maintained at constant temperatures that differ by ΔT. The temperature T of the fluid is measured in units of ΔT, and is considered to be decomposed into mean and fluctuating parts: $T = \bar{T} + \theta$, where the overbar denotes horizontal average. All variables are made dimensionless by using the plate separation d and the thermal diffusion time d^2/κ as units of length and time, where κ is the thermal diffusivity of the fluid.

As in I, the velocity $\mathbf{u}$ and the temperature fluctuation θ are expanded in terms of a set of planform functions $f_i(x, y)$ of the horizontal Cartesian coordinates:

$$\mathbf{u} = \sum_i \left(a_i^{-2} \frac{\partial f_i}{\partial x} \frac{\partial W_i}{\partial z}, \; a_i^{-2} \frac{\partial f_i}{\partial y} \frac{\partial W_i}{\partial z}, \; f_i W_i \right), \tag{2.1}$$

$$\theta = \sum_i f_i \Theta_i, \tag{2.2}$$

where the horizontal wavenumbers a_i are constants and the amplitude functions W_i, Θ_i depend on the vertical coordinate z and time t. The planforms f_i satisfy

$$\frac{\partial^2 f_i}{\partial x^2} + \frac{\partial^2 f_i}{\partial y^2} = -a_i^2 f_i, \tag{2.3}$$

$$\overline{f_i f_j} = \delta_{ij}, \tag{2.4}$$

and could be chosen to form a complete set, though here we consider only two or three terms in the series (2.1) and (2.2). Thus the horizontal structures of the fluctuating fields are quite crudely represented, but the representation by W_i and Θ_i of the vertical structures and time dependence is computed with some care. Note furthermore that the form (2.1) chosen for the velocity, which automatically satisfies div $\mathbf{u} = 0$, does not include terms representing flow with vertical vorticity.

The equations governing the model, whose derivation was described in I, are

$$\frac{1}{\sigma} \mathscr{D}_i \left(\frac{\partial W_i}{\partial t} \right) + \frac{1}{\sigma} \sum_{j,k} \frac{C_{ijk}}{(a_j a_k)^2} \{ a_{kij} W_k \mathscr{D}_j D W_j + (a_{kij} + a_{ijk}) (D W_k) \mathscr{D}_j W_j \}$$
$$= -Ra_i^2 \Theta_i + \mathscr{D}_i^2 W_i, \tag{2.5}$$

Class	Notation	Description†
1	(F, 2)	Two aligned hexagons
2	{F, $\sqrt{3}$}	Two rotationally displaced hexagons
3	[F, 2]	Two aligned squares
4	{F, $\sqrt{3}$, 2}	A hexagon and its first two overtones
5	(F, n, $n+1$)	A triad of three aligned hexagons

† See appendix A for a more-detailed description.

TABLE 1

$$\frac{\partial \Theta_i}{\partial t} + \sum_{j,k} \frac{C_{ijk}}{(a_i a_k)^2} \{a_{ijk} \Theta_j D W_k + 2a_1^2 a_k^2 W_k D\Theta_j\} = -W_i D\overline{T} + \mathscr{D}_i \Theta_i, \tag{2.6}$$

$$\frac{\partial \overline{T}}{\partial t} + \sum_j D(W_j \Theta_j) = D^2 \overline{T}, \tag{2.7}$$

where

$$D \equiv \frac{\partial}{\partial z}, \quad \mathscr{D}_i \equiv D^2 - a_i^2, \quad a_{ijk} \equiv a_i^2(a_j^2 + a_k^2 - a_i^2), \quad C_{ijk} \equiv \tfrac{1}{2}\overline{f_i f_j f_k}. \tag{2.8}$$

The lower ($z = 0$) and upper ($z = 1$) boundaries are treated as rigid perfect thermal conductors. Thus we impose the conditions

$$W_i = DW_i = \Theta_i = 0 \quad (z = 0, 1), \tag{2.9}$$

$$\overline{T} = 1 \quad (z = 0), \quad \overline{T} = 0 \quad (z = 1),$$

along with suitable initial conditions, which we shall discuss later.

In most cases we consider combinations of modes for which the interaction parameters C_{ijk} do not all vanish when i, j and k are not equal. Such combinations must have wavenumbers a_i that satisfy certain selection rules. The various classes studied are discussed explicitly in appendix A; they are summarized in table 1. We shall refer to the mode with lowest wavenumber as the fundamental, and the others as horizontal overtones, and characterize a mode combination by the symbol F together with parameters that define the overtone wavenumbers in terms of the fundamental.

As in the case of the single-mode representation, multimode solutions exist in pairs. Two members of such a pair have the same Nusselt number N, and each can be derived from the other by the transformation

$$z \to 1 - z, \quad W_i \to -W_i, \quad \Theta_i \to -\Theta_i, \quad \overline{T} \to 1 - \overline{T}. \tag{2.10}$$

In the remainder of this discussion we shall regard any two steady states that are related by this transformation as being equivalent.

We now turn to some important derived quantities. The first of these is the total heat flux $F(z, t)$, which, when measured in units of the flux in the conductive state, is given by

$$F = \sum_j W_j \Theta_j - D\overline{T}. \tag{2.11}$$

For steady solutions, F is independent of z and is equal to the Nusselt number N, as it is normally defined. For time-periodic solutions the time average of F over one period is independent of z, and we call this average the Nusselt number. For the aperiodic solutions we have obtained, the temporal averages of F always tended to

a constant limit for long averaging times. Hence, for such cases, we may define a Nusselt number as

$$N = \lim_{s\to\infty} s^{-1} \int_0^s F(z,t)\,dt, \tag{2.12}$$

which is independent of z. A second derived quantity of interest is the horizontal average of the specific kinetic energy associated with each mode:

$$E_i(t) = \frac{1}{2}\int_0^1 [a_i^{-2}(DW_i)^2 + W_i^2]dz. \tag{2.13}$$

To facilitate comparison with experimental data, it is useful to define also the r.m.s. velocity and temperature. For this purpose we introduce the operation $\langle\ \rangle$, which represents an average over horizontal coordinates and time. The r.m.s. vertical velocity is

$$w_{\rm rms} \equiv \langle w^2\rangle^{\frac{1}{2}} = \left\{\lim_{s\to\infty} s^{-1}\int_0^s \sum_j W_j^2\,dt\right\}^{\frac{1}{2}}, \tag{2.14}$$

with a similar expression for the r.m.s. temperature fluctuation $\theta_{\rm rms}$. We also consider the time-averaged mean temperature field

$$\langle T\rangle = \lim_{s\to\infty} s^{-1}\int_0^s \bar{T}(z,t)\,dt. \tag{2.15}$$

The partial differential equations (2.5)–(2.8) have been solved by the finite-difference methods that are discussed in appendix A of II. We outline them briefly here. All spatial derivatives are expressed by second-order-accuracy centred differences. To ensure adequate spatial resolution, a stretched computational mesh is used. When introducing the stretching and also in displaying some of our results, it is useful to define a new independent variable $\xi(z)$ in which the grid points are evenly spaced. The mapping between ξ and z is usually based on cubic or arctangent functions, with the stretching parameters so chosen that boundary layers can be resolved accurately (see also Gough, Spiegel & Toomre 1975*b*). Implicit time representations are used in which all differential spatial operators are evaluated at the same time levels, ranging from a time-centred scheme, which minimizes numerical diffusion, to the very stable but diffusive fully implicit scheme. In addition, provision is made to deal directly with the time-independent equations when sequences of steady solutions are to be constructed.

The resulting nonlinear difference equations are solved at each time step by Newton–Raphson iteration, which requires repeated inversion of a $M\times M$ block-tridiagonal matrix. The number M of spatial grid points is usually about 300. The blocks are of order $J\times J$, with J depending upon the number of modes retained in the analysis; $J = 7$ for two modes and $J = 10$ for three modes. Four Newton–Raphson iterations are usually needed per time step to solve the finite-difference equations with a relative precision of about 10^{-14}. For a three-mode truncation each time step requires 4·5 s of machine time on an IBM 360/95.

The results presented in this paper are based on over five hundred multimode solutions sampling the (R,σ,a_i) parameter space. Yet these have given us only a coarse coverage of the various kinds of behaviour of the modes. The investments in computer time are particularly high when it is required to ascertain the nature of the time dependence in some of the solutions. Only with very fine temporal and spatial resolution can the periodic solutions be obtained. We used about 200 time steps per periodic cycle for the {F, $\sqrt{3}$} solution illustrated in figure 3, and about 50 time steps per cycle for the gentler evolution of the {F, $\sqrt{3}$, 2} solution in figure 4. If started

from a steady solution near by, these solutions attain their periodic behaviour within about 10 cycles of computation. Although numerical errors can readily perturb a periodic solution into an aperiodic one, there also exist solutions that appear to be genuinely aperiodic or nearly periodic with long-term modulation.

A variety of initial conditions were used in the calculations: They were usually constructed from solutions with different R, σ and a_i, but often the amplitudes were scaled, and their relative signs changed, and random noise added, in order to test whether the final states to which the solution evolve depend on initial conditions. The steady and periodic solutions, when they exist, are generally insensitive to the initial conditions and are stable, but of course there are special regions in state space where this is not so.

3. Survey of solutions

We have toured a region of parameter space to descry the most common features of the solutions; the region extends in R to a maximum value of 10^7, in σ it ranges from 10^{-2} to 10^4, and it covers the entire range of wavenumbers within which convection is sustained. Here we summarize the results, confining our report to two- and three-mode representations.

When $R \leqslant 1707$ our solutions always evolved to the conductive state. Convective solutions at slightly supercritical Rayleigh numbers are dominated by just one of the modes, whose structure is close to that of a corresponding single-mode solution. It is not until R exceeds about 10^5 that the multimode representation becomes richer than the single-mode case. We therefore focus our attention on the range $10^5 \leqslant R \leqslant 10^7$.

We have encountered steady, periodic and aperiodic solutions. We call steady solutions those that evolve to steady states as $t \to \infty$, and these seem to be the most prevalent if all regions in parameter space are weighted equally. Solutions that appear to remain time-dependent for all time occupy a narrow wavenumber range. In practice it was usually easy to decide whether or not a solution is time-dependent; difficulty was encountered only near the borders of the domains of time dependence, where the solutions evolve very slowly. We have not attempted to define these borders precisely. The time dependence is often complicated, and we have concentrated on the periodic cases, being content for the moment to note where in parameter space the apparently chaotic behaviour seemed to arise.

3.1. *Steady two-mode solutions*

A close-packed cellular solution of the full equations of motion can be obtained by a modal expansion if sufficiently many terms in the expansion are kept. How many modes are needed to achieve reasonable accuracy should be decided by increasing the number until the result stops changing. Our two-mode solutions give some indication of the accuracy of the one-mode solutions at moderate Rayleigh numbers.

In figure 1 comparison is made between the Nusselt numbers of a one-mode hexagon obtained in II and two directly coupled steady two-mode solutions. The parameters chosen are $R = 10^5$ and $\sigma = 1$, and N is plotted as a function of wavenumber. Every solution shown corresponds to the gravest vertical mode of linear theory, as do all the steady states we obtained from time integrations, even when initial conditions close to steady vertical overtone solutions were chosen. The dashed curve corresponding to the one-mode case has a single maximum at $a = a_m$, here 6·6, in common with all other one-mode solutions. The principal result in figure 1 is the

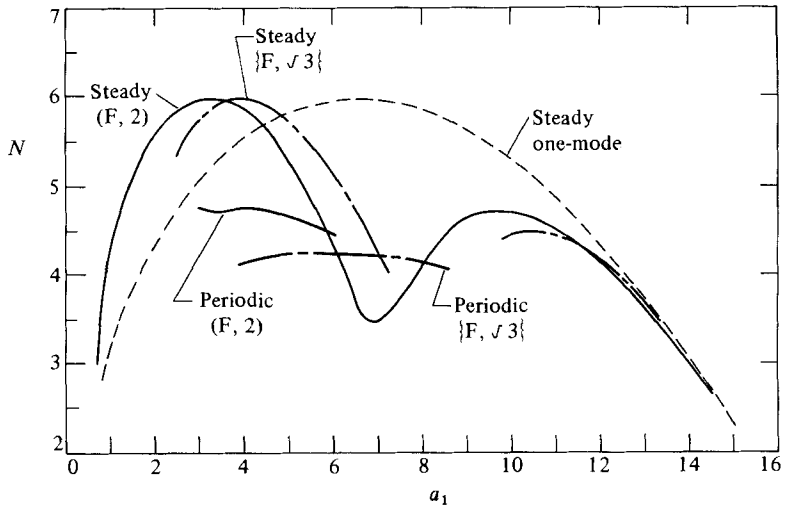

FIGURE 1. Nusselt numbers of steady one- and two-mode solutions at $R = 10^5$, $\sigma = 1$, plotted against wavenumber. The dashed line is for a single hexagon ($C = 6^{-\frac{1}{2}}$). The solid curve is for a hexagon and its aligned overtone (F, 2) and the dot-dashed line for a hexagon and its rotated overtone {F, $\sqrt{3}$}. In these cases the abscissa is the wavenumber a_1 of the fundamental mode. Convection is possible provided that $a_2 > \tilde{a}_1$ and $a_1 < \tilde{a}_2$, where $(\tilde{a}_1, \tilde{a}_2) = (3{\cdot}2 \times 10^{-3}, 31{\cdot}3)$ is the wavenumber range of linear instability of the conductive state. No other stable steady solutions were found for these values of R and σ. Nusselt numbers of the time-periodic solutions are also shown for the two cases, the solid and dot-dashed lines referring to (F, 2) and {F, $\sqrt{3}$} as before; when a_1 was outside the ranges over which these lines extend, solutions tended always to steady states. No aperiodic solutions were found.

solid curve, indicating N for a hexagon corrected by its first aligned overtone. The most striking feature is the existence of two maxima, which is typical of solutions with $\sigma \gtrsim 1$. Also shown are values of N for the same fundamental hexagon with its rotated overtone.

To appreciate the significance of the two-mode results one must realize that when $a_1 \lesssim a_m$ the fundamental has much smaller amplitude than the overtone. (We use the maximum of $W_i(z)$ as a measure of amplitude.) Therefore when $a_1 \lesssim a_m$ the steady two-mode solutions resemble the one-mode solutions with wavenumbers equal to a_2. If the steady branches of the solid and dot-dashed curves in this range are stretched horizontally by factors 2 and $\sqrt{3}$ respectively, they become almost identical with the one-mode curve. The slight differences arise because mode 2 is modulated by mode 1, which plays the role of a subharmonic.

At higher wavenumbers the flow becomes dominated by the fundamental. The transition is quite abrupt, and occurs just above $a_2 = 12$ in both cases. The amplitude of the overtone then decreases with increasing a_1, and the second maximum in the Nusselt number corresponds to a maximum in the heat transport by the fundamental mode. This does not occur near $a_1 = a_m$, however, because here the amplitude of the overtone is still substantial, even though it is either stable or only slightly unstable in linear theory. It owes its existence to the fundamental, from which it drains energy. As a_1 increases, the overtone develops nodes in its vertical structure, thus increasing the rate at which it dissipates energy. At even higher wavenumbers its amplitude diminishes so much that its dynamical influence on the fundamental mode becomes negligible; thus the two-mode curves in figure 1 eventually join the one-mode curve.

The introduction of a third mode raises the number of steady solutions. Since we

find that the correction to the mean quantities caused by an additional mode are not appreciable for the steady solutions when $R \sim 10^5$, we have not studied these in detail. The matter is quite different for the time-dependent solutions, which have no counterpart in one-mode theory. In the case of hexagons, the fundamental mode has two first overtones, and we consider it natural, though not compelling, to include them both.

A point that deserves comment is that the Nusselt number of the steady hexagonal solutions decreases as the Prandtl number decreases, as is the case for the single-mode solutions. However, numerical solutions of the full equations for axisymmetrical convection in a cylinder by Jones, Moore & Weiss (1976) show very little σ-dependence, and even a slight increase in N as σ decreases. The reason is that the flow organizes itself in such a way as to diminish the restraining effect of the advection, as in the case of rolls. As was first noticed by J. Herring (unpublished) for convection in a horizontally unbounded layer at the limit $\sigma = 0$, this permits the energy of the motion to exceed the potential energy associated with the unstable stratification, and it leads to a form of two-dimensional convection that Moore & Weiss (1973) have likened to a flywheel. We pointed out in II that the constraints imposed on the flow by severe modal truncation prevent the annihilation of the effects of advection, even when we attempt to represent axisymmetrical convection in a cylinder. This underlines a deficiency in the model. Nevertheless, that may not necessarily be of great concern for modelling real flows, because the flywheel solutions are unstable (Jones & Moore 1979). We believe that the development of the instabilities will diminish N when σ is very low.

3.2. *Time-dependent solutions*

Our surveys were conducted in limited regions of parameter space. We have done very little work with more than three modes, and will not report at all on that. And, in our three-mode studies, we have confined our attention almost exclusively to hexagonal planform functions. Thus we report mainly on them, mentioning more briefly the related two-mode solutions.

Provided R and σ are sufficiently high and there is at least one non-zero component of C_{ijk} with i, j and k not all equal, time-dependent multimode solutions can be found within a limited range of wavenumbers. The extent of the wavenumber range increases as R increases. When $R \leqslant 10^4$ only steady solutions could be found whatever the value of σ; and at $R = 10^5$ periodic two-mode solutions were obtained, as indicated in figure 1. At $R = 10^5$ all our three-mode solutions were steady, and when R was high enough for time dependence to occur the motion was more ordered than the two-mode solutions. Some features of these solutions are listed in table 2.

We have found no aperiodic solutions with $\sigma \geqslant 6{\cdot}8$ and $R < 10^7$. There is some diversity in the forms of the periodic solutions, though usually the flow is dominated by the fundamental mode. Yet an important contribution to the activity comes from the overtone modes, for without them sustained time dependence is impossible. For some solutions the response of the fundamental is a change in sign of W_1 everywhere, signifying a reversal in the flow direction, whereas for others it is merely a large fluctuation in the speed of circulation in the cell. Examples of such solutions are illustrated in figures 2–4.

The time evolution of a periodic solution for a hexagon and its aligned overtone (F, 2) is represented in figure 2 (*a*) by the mean temperature $\overline{T}$ and the amplitude W_1, W_2 of the vertical components of velocity of the two modes. Here $R = 10^6$, $a_1 = 10$ and $\sigma = 6{\cdot}8$. The periodic solutions at $R = 10^5$ and $R = 5 \times 10^5$ are similar. In this

			$\sigma = 1$			$\sigma = 6{\cdot}8$		
R	Class	a_1	N	$\Delta F_b/N$	P	N	$\Delta F_b/N$	P
10^5	1: (F, 2)	2·0	*5·6*	—	S	—	—	—
		3·0	4·8	0·9	0·31	—	—	—
		3·5	4·7	0·8	0·22	—	—	—
		4·0	4·8	0·8	0·18	*6·0*	—	S
		5·0	4·7	0·8	0·15	4·4	0·6	0·16
		6·0	4·5	0·9	0·17	4·2	0·5	0·13
		6·5	*3·7*	—	S	—	—	—
		8·0	*4·1*	—	S	*4·8*	—	S
	2: {F, $\sqrt{3}$}	3·5	*5·9*	—	S	—	—	—
		4·0	4·1	1·0	0·26	—	—	—
		5·0	4·2	0·9	0·21	—	—	—
		6·0	4·2	0·9	0·18	*4·5*	—	S
		7·0	4·2	1·2	0·17	—	—	—
		8·0	4·1	1·4	0·21	4·1	0·7	0·18
		8·5	4·1	1·5	0·26	—	—	—
		9·0	*4·3*	—	S	*4·4*	—	S
	3: [F, 2]	4·0	*3·3*	—	S	—	—	—
		5·0	3·3	—	0·14†	*4·5*	—	S
		6·0	3·4	—	0·15	*4·2*	—	S
		8·0	*3·9*	—	S	—	—	—
5×10^5	1: (F, 2)	4·0	—	—	—	8·0	0·1	0·014
		6·0	*10·2*	—	S	8·1	0·1	0·012
		8·0	7·0	0·6	0·099	7·3	0·1	0·013
		10·0	*6·1*	—	S	6·4	0·5	0·019
10^6	1: (F, 2)	2·0	*10·4*	—	S	—	—	—
		4·0	10·1	0·2	0·0090	*12·3*	—	S
		6·0	10·3	0·1	0·0080	11·4	0·2	0·0057
		8·0	10·1	0·2	0·0084	11·0	0·1	0·0050
		10·0	9·2	0·2	0·0092	10·0	0·2	0·0059
		12·0	8·0	0·4	0·013	9·2	0·3	0·0217
		14·0	*7·1*	—	S	*8·1*	—	S
	2: {F, $\sqrt{3}$}	12·0	—	—	S	—	—	—
		14·0	7·6	0·1	0·0033‡	6·4	0·2	0·0096‖
		16·0	7·6	1·0	0·038	8·4	0·7	0·028
		18·0	7·8	1·0	0·075	—	—	—
		20·0	*8·5*	—	S	—	—	—
	3: [F, 2]	6·0	11·0	0·6	0·0104†	—	—	—
		8·0	10·8	0·3	0·0083	—	—	—
		10·0	10·1	0·3	0·0073	—	—	—

continued on facing page

example, the overtone mode has roughly half the amplitude of the fundamental, and represents two superposed layers of cells, always oriented such that fluid leaves the walls in plumes. The oscillation of the fundamental cell is accomplished by the formation of countercells in the thermal boundary layers, which grow at the expense of the main cell, eventually destroying it and merging to form a single cell whose flow is oppositely directed to that of the original cell. The process then repeats to restore the original state. The second half of the cycle is essentially the same as the first, since in this case the solution at any instant can be derived from the solution half a period earlier by the transformation (2.10). Thus there are two maxima per period in the

			$\sigma = 6{\cdot}8$			$\sigma = 200$		
R	Class	a_1	N	$\Delta F_b/N$	P	N	$\Delta F_b/N$	P
	4: {F, $\sqrt{3}$, 2}	10·0	*11·3*	—	S	*11·3*	—	S
		12·0	*10·4*	—	S	10·3	0·1	0·0098
		14·0	9·5	0·5	0·012	9·3	0·5	0·0088
		16·0	*8·9*	—	S	*8·8*	—	S
10^7	1: (F, 2)	6·0	25·6	0·1	0·0018‡	—	—	—
		15·0	20·8	0·1	0·0030‡	—	—	—
	4: {F, $\sqrt{3}$, 2}	14·0	*26·0*	—	S	—	—	—
		15·0	25·3	0·4	0·0143§	25·5	0·2	0·0068
		20·0	*23·8*	—	S	23·1	0·3	0·0077
		24·0	—	—	—	17·9	0·7	0·0082‡

TABLE 2. Properties of time-dependent multimode solutions. The modal configurations are identified by class in the second column (see table 1) and in the third column by the wavenumber a_1 of the fundamental mode. Tabulated for each value of the Rayleigh number R and Prandtl number σ are the Nusselt number N, the relative heat flux variation $\Delta F_b/N$, where ΔF_b is the difference between the greatest and least values of the heat flux at either boundary, and the oscillation period P. In cases where $\Delta F_b/N \gtrsim 0{\cdot}2$, substantial excursions of E_b from the mean occur during relatively short intervals of time. Nusselt numbers for steady solutions are in italics. In order to give an idea of the range of wavenumbers within which time-dependent solutions exist, we indicate, when we have the information, where solutions tend to steady states (with the symbol 'S'). Note that the three-mode entries under $\sigma = 6{\cdot}8$ and $\sigma = 200$ actually have $\sigma = 200$ and $\sigma = 10^4$.

† The periods quoted for squares are the complete periods of oscillation of the flow; the heat flux varies with half that period.

‡ The oscillations are not strictly periodic, but are modulated slightly on a timescale longer than the periods quoted.

§ Each period consists of two similar oscillations of the flow, which are executed in a time interval of about 0·007.

‖ The solution suffers occasional irregularly spaced bursts.

heat flux at the boundaries, illustrated in figure 2(*b*). The symmetry between the two halves of the cycle is typical of the (F, 2) solutions.

Figure 3(*a*) depicts the time evolution of a solution of a hexagon and its rotationally displaced overtone: type {F, $\sqrt{3}$}. Here $a_1 = 16$, and again $R = 10^6$ and $\sigma = 6{\cdot}8$. The principal difference between this solution and that for (F, 2) is that here the period is about four times longer and mode 2 shows more convolutions in its structure. The configuration in which the flow is most commonly found is one in which the fundamental has no interior zero and the overtone has one. The reversal in mode 1 is accomplished by the growth of a single countercell near one of the boundaries, this having just occurred near the upper boundary (to the right) at the beginning of the time sequence illustrated in figure 3(*a*). The countercell grows in amplitude and extent, generating a large heat flux at the boundary from which it grew, and eventually displaces the original cell. Subsequently the flow relaxes thermally, the overall kinetic energy of the motion decreases, and the boundary layers in $\bar{T}$ enlarge until the lower boundary layer becomes unstable to the growth of a countercell. The second half of the cycle is just like the first, being derivable from it by the transformation (2.10). This solution exhibits variations in the heat flux at the boundaries, shown in figure 3(*b*), that have considerably greater amplitude than in the previous (F, 2) case.

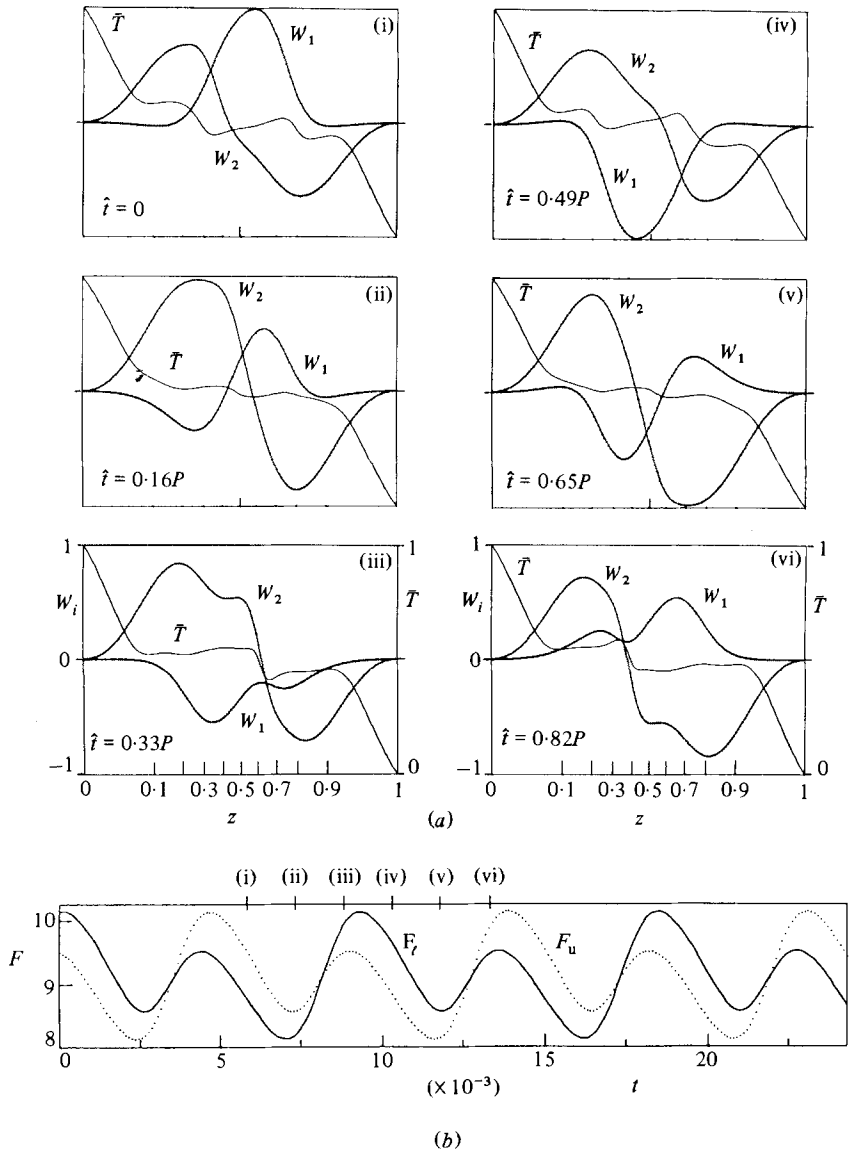

FIGURE 2. (*a*) Mean temperature $\bar{T}$ and velocity amplitudes W_1, W_2 for a hexagon and its aligned overtone (F, 2). $R = 10^6$, $\sigma = 6{\cdot}8$, $a_1 = 10$, $N = 9{\cdot}20$. W_1 and W_2 are plotted in units of their maximum values, 310 and 174 respectively. The abscissa is marked at intervals of 0·1 in z. The solution is periodic in t with period $P = 9{\cdot}2 \times 10^{-3}$, and the panels are at six uniformly spaced times $\hat{t}$, which is simply time measured from the first panel. For most of the time W_1 has the same sign everywhere, as in (i), (iii), (iv) and (vi); the transitions, which are captured in (ii) and (v), are quite abrupt. We have found similar periodic solutions at $R = 10^5$ and 5×10^5. (*b*) Time variation of the heat fluxes F_ℓ (solid line) and F_u (dotted line) at the lower and upper plates. The times $\hat{t}$ associated with the six panels in (*a*) are marked on the upper border of the panel. The boundary fluxes are related by $F_u(t) = F_\ell(t + \frac{1}{2}P)$. The solution in the second half of a cycle is derivable from that in the first half by the transformation (2.10). This is a property of all our two-mode solutions. Two interacting squares are superficially similar to this case, and possess the additional symmetry, never found in the hexagon solutions, of having the fundamental mode spatially symmetrical about $z = \frac{1}{2}$ and the overtone antisymmetrical. In that case $F_u(t) = F_\ell(t)$, and the period of the heat-flux oscillations is half that of the oscillation of the flow.

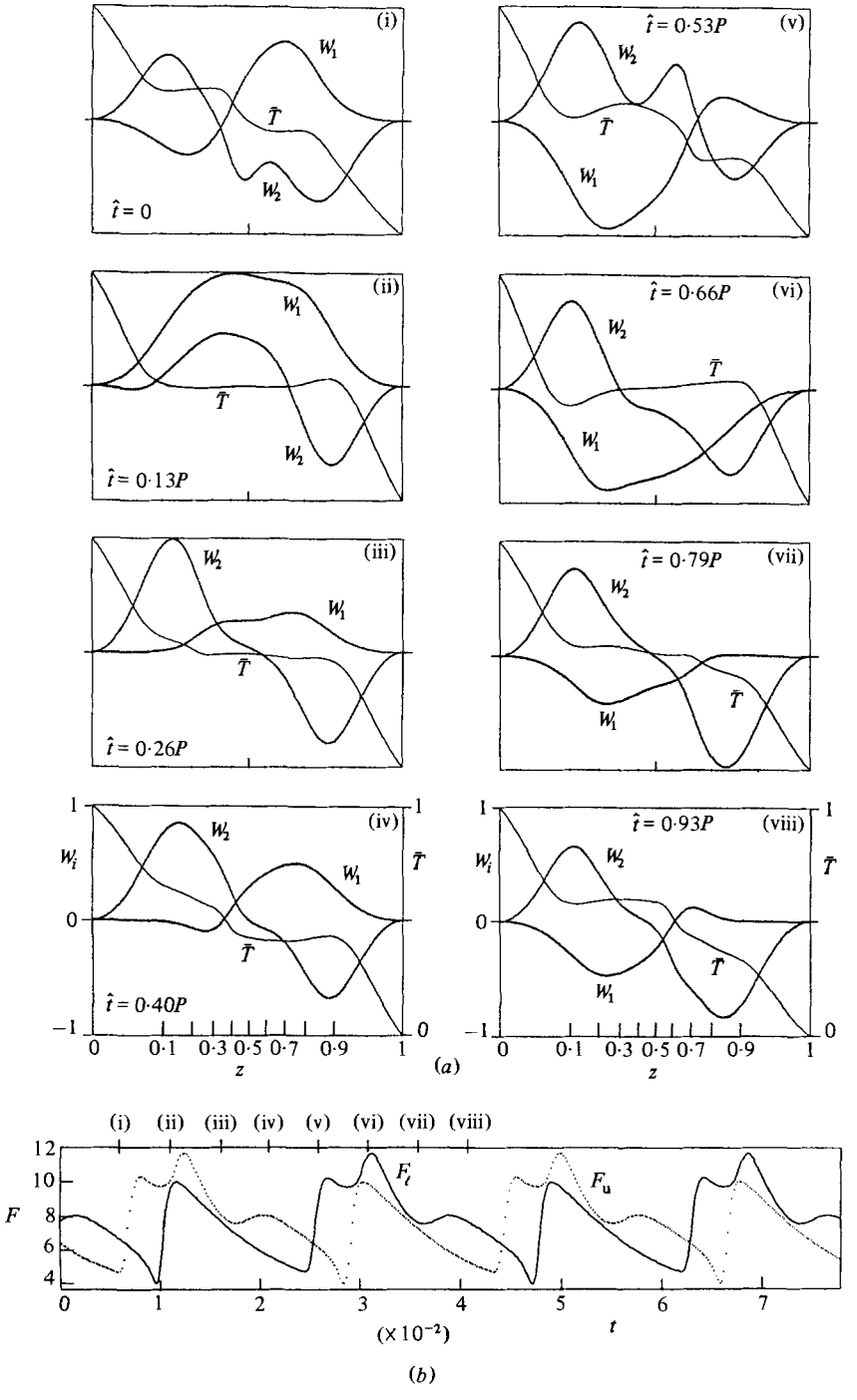

FIGURE 3. Similar to figure 2, showing a hexagon and its related overtone {F, $\sqrt{3}$}. $R = 10^6$, $\sigma = 6{\cdot}8$, $a_1 = 16$, $N = 7{\cdot}62$ and $P = 3{\cdot}78 \times 10^{-2}$. The degree of stretching of the z-scale is the same as in figures 2 and 4. W_1 and W_2 are plotted in units of their maximum values, 296 and 72 respectively.

An example of a three-mode time-dependent periodic solution is shown in figure 4 for a hexagon and its two principal horizontal overtones, of type {F, $\sqrt{3}$, 2). The left panels of figure 4(*a*) are plots of $\bar{T}$ and W_i ($i = 1, 2, 3$) as functions of z at uniformly separated times through one period of the solution. The right panels show the total heat flux F and temperature fluctuation amplitudes Θ_i at the same times. The parameters are $R = 10^6$, $\sigma = 6{\cdot}8$ and $a_1 = 14$. The wavenumber is in the middle of the fairly narrow range in which time dependence is found at these values of R and σ. Since $N = 9{\cdot}48$, a non-uniform z-scale has been chosen so that the structures of the boundary layers may be seen.

The solution illustrated in figure 4 is dominated by the fundamental, which contains ten times more kinetic energy than the overtones and transports most of the heat. The fundamental (mode 1) is modulated in amplitude by the overtones, but it does not reverse sign, as is also the case for the aligned overtone (mode 3). It is the rotated overtone (mode 2) that exhibits the most complicated behaviour, but it has the least kinetic energy and so has only a small direct effect on the heat flux. Some aspects of the relative importance of the velocity variation in different modes may be seen in figure 4(*b*). Each overtone experiences variations in kinetic energy of about $1{\cdot}5 \times 10^2$. This is a modest perturbation on the energy of the aligned overtone, but it is comparable to the mean kinetic energy of the rotated overtone. The energy of the fundamental is about 10^4, and its fluctuations are comparable to this. Hence we conclude that the principal source of temporal variation in the fundamental is its interaction with the mean field, though the presence of at least one of the overtones is essential.

In figure 4(*c*) is shown the time dependence of the heat flux at the two boundaries. The amplitude of the variation is 20 %. In contrast, as can be seen in the right panels in figure 4(*a*), large temporal variations in the heat flux F occur in the body of the fluid. Two-mode solutions have a similar property. In this example, the maximum (in z) vertical heat flux varies between 3 and 23. Such thermal bursts are a common feature of our time-dependent solutions.

To picture the flow pattern as it might look to a numerical experimenter, we have used contour plots of the vertical velocity. In figure 5 we present shaded versions of such plots for the same four times as in figure 4(*a*). The view shown is of the boundary layer, at $z = 0{\cdot}05$. The velocity is upward in the darker regions. The appearance of figure 5 is insensitive to location in the boundary layer and is similar for the other boundary layer. A comparable picture for the vertical velocity in the interior would look much more like a one-mode pattern, though the small-scale structure remains discernible. The individual frames in figure 5 show that there is a transition in the time evolution between the domination of the small-scale structure with characteristic horizontal scale $2\pi/2a_1$ and the large-scale structure with scale $2\pi/a_1$. When small scales dominate, the flow consists of isolated rising plumes. When the large scales preponderate, the hexagonal structure is more pronounced. An interesting feature of the large-scale flow is that the eye tends to pick out hexagons with vertices at the centres of the six fundamental modes immediately surrounding some particular mode. Thus there is a rising column of fluid at the centre and spokes of rising fluid radiating to the vertices. The visual scale appears to change by a factor 4 during the course of the time dependence, even though the greatest and least wavenumbers of the planforms differ by a factor of only 2.

Returning to the structure of the solutions, we show in figure 6 the time-averaged r.m.s. temperature and velocity fields for the three-mode example illustrated in figures 4 and 5. The results are not dissimilar to those of comparable one-mode

solutions presented in II. In particular, the midplane mean temperature is not equal to $\frac{1}{2}$, and the vertical velocity achieves its maximum closer to the boundary towards which the central column of the hexagon is flowing.

These results are fairly characteristic of our three-mode periodic solutions. At $R = 10^6$ all the time-dependent three-mode solutions we investigated were periodic, but at $R = 10^7$ periodic solutions were found only for $\sigma \gtrsim 200$. Time variations generally become smoother as σ is increased above unity. Two-mode solutions are also periodic at high σ, and if $R \gtrsim 5 \times 10^5$ they are aperiodic when $\sigma \simeq 1$. The transition occurs at higher values of σ for higher R. The nature of the aperiodic solutions is complicated and varied. We suspect that some of these solutions alternate irregularly between two nearly periodic flows having different periods. Other aperiodic solutions are more chaotic and possess no discernible systematic variation in time. At even lower values of σ the two-mode solutions are again periodic, but the flow is very different from the high-σ solutions. The region is divided into two convecting layers separated by a diffusive interface, which moves from one plate to the next and then returns. We suspect that this behaviour is a consequence of our having an overrestricted representation of the flow. At the lowest value of σ we investigated ($\sigma = 10^{-2}$) solutions were steady, and usually several stable states could be found for given values of R and a_1.

4. High overtones

Our choice of the lowest overtones in the two- and three-mode studies of §3 was motivated by the wish to obtain improved dynamical descriptions of flow in a single cell. But evidence exists for the importance of diverse scales of motion in fixing the heat flux at very high Rayleigh number. Convection in the sun shows cell-like structures on disparate horizontal scales. And recent experiments by R. Krishnamurti (1980, private communication) show qualitatively similar structures. Within the context of the present description, we have argued (reported in Spiegel 1971) that modes confined in the boundary layer created by the fundamental produce marked changes in the total Nusselt number. The picture is like that in the flows used to maximize heat flux by Busse (1969) and Chen (1971). In this section we attempt to quantify these ideas by reporting on three-mode solutions in which the overtones have relatively high wavenumbers, in some cases high enough so that their horizontal scales are as small as the thickness of the principal boundary layer.

To force the small scales by advection terms, we chose triads of hexagons for which $C_{ijk} \neq 0$, and confined our attention to aligned hexagons. This is case (F, n, $n+1$) described in appendix A. The wavenumber a_1 is of order unity and the value of n is of the order of the Nusselt number N as calculated by one-mode theory at a wavenumber a_1. One question that especially interested us was whether the amplitude of the overtones would indeed be preferentially high in the boundary layers. Unfortunately, we found that there is not a simple answer to this question and that the number of possibilities is large. We shall therefore simply attempt to outline some of these.

We concentrate on $R = 10^7$, which is large but still manageable numerically. We discuss only $\sigma = 10$, $a_1 = 3$, and let a_2 vary from 15 to 114. Throughout this entire range we found stable steady solutions and, except for the highest values of a_2, several such solutions exist. When $a_2 > 78$ the amplitudes of the overtones were imperceptible. For $74 < a_2 < 78$ only the lower overtone is excited. For $a_2 > 60$ both overtones are concentrated near boundaries. Sometimes each is concentrated near to a single

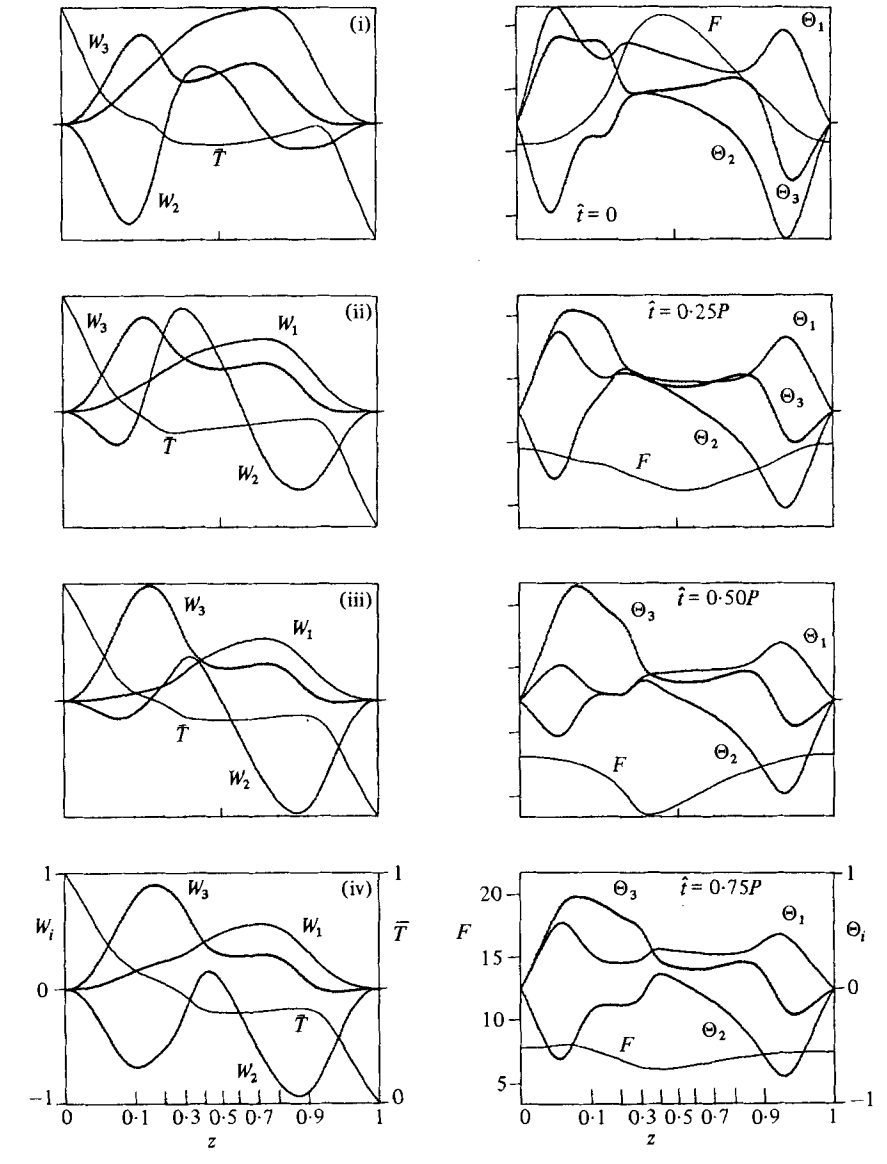

(*a*)

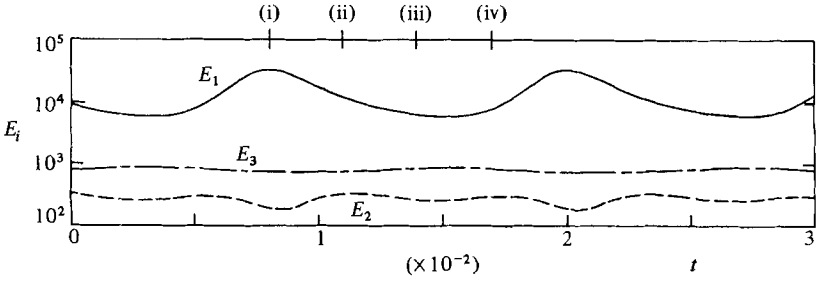

(*b*)

FIGURE 4 (*a*, *b*). For caption see facing page.

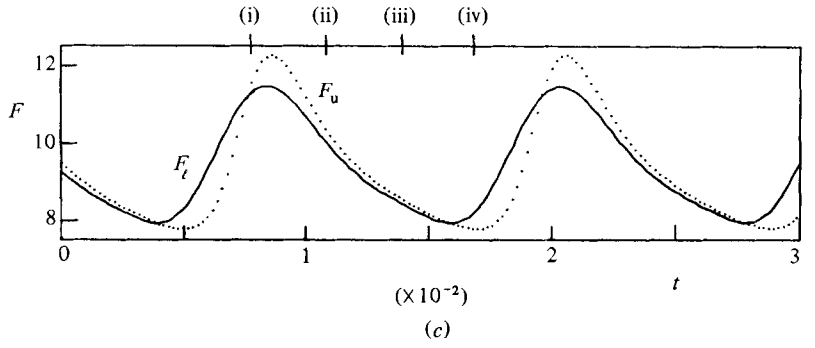

FIGURE 4. (*a*) A periodic three-mode hexagon solution {F, $\sqrt{3}$, 2}. $R = 10^6$, $\sigma = 6{\cdot}8$, $(a_1, a_2, a_3) = (14, 24{\cdot}2, 28)$, $N = 9{\cdot}48$ and $P = 1{\cdot}20 \times 10^{-2}$. The left panels are the mean temperature $\bar{T}$ and velocity amplitudes W_i, plotted as functions of z at four equally spaced times during one period. The right panels are the total heat flux F and the temperature fluctuation amplitudes Θ_i. W_1, W_2 and W_3 are scaled by their respective maxima: 321, 46 and 84; and Θ_1, Θ_2 and Θ_3 similarly by 0·122, 0·094 and 0·094. The abscissa is marked at intervals of 0·1 in z; the stretching of the scale is the same in all panels, and is identical with that in figures 2 and 3. (*b*) Kinetic-energy contributions $E_i(t)$ of the three modes illustrated in (*a*). The origin of time is the same as in (*a*). The times $\hat{t}$ of the four sets of panels in (*a*) are indicated on the upper border. (*c*) The heat fluxes $F_\ell(t)$ (solid line) and $F_u(t)$ (dotted line) at the lower and upper plates.

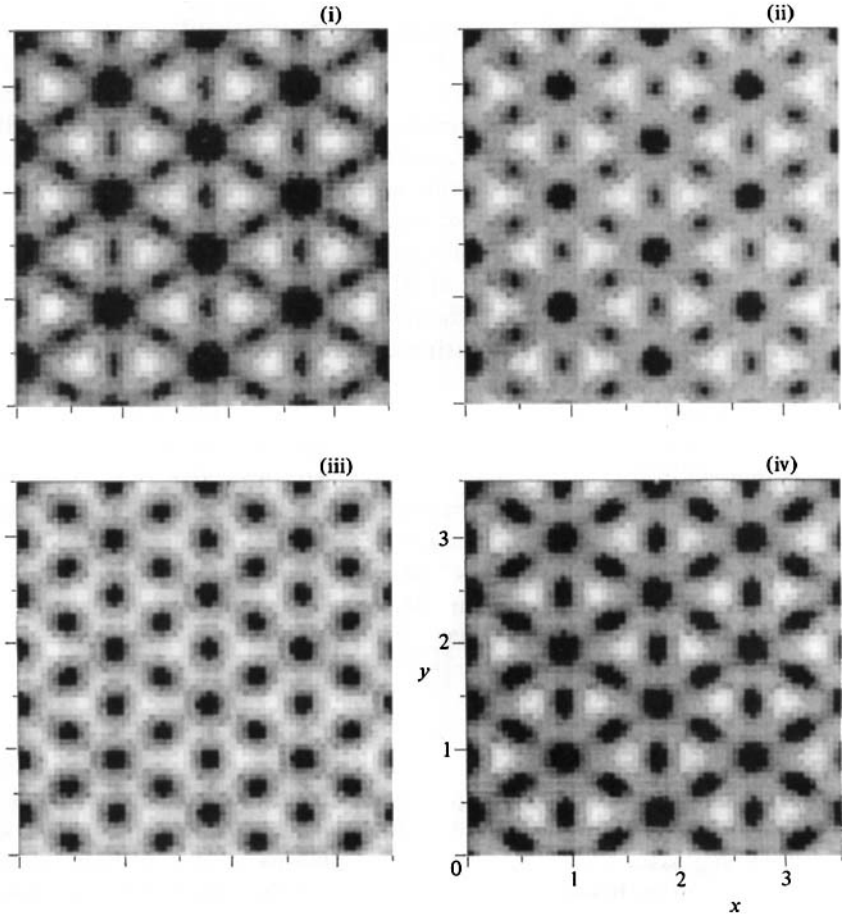

FIGURE 5. Contours of vertical velocity amplitude evaluated on the horizontal plane at $z = 0{\cdot}05$ for the four solutions shown in figure 4(*a*). Here the velocity is upwards in the darker regions, downwards in the lighter regions.

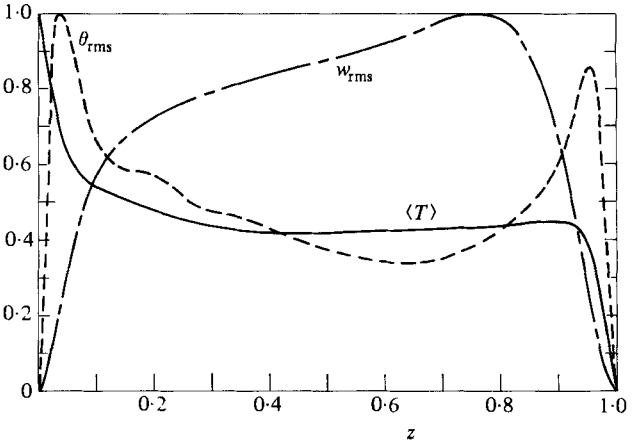

FIGURE 6. The average over one period of the r.m.s. velocity and temperature fluctuations, and the time-averaged mean temperature for the solution illustrated in figures 4 and 5, plotted on a uniform scale against z. The amplitudes $w_{\rm rms}$, $\theta_{\rm rms}$, and $\langle T \rangle$ are defined by (2.14) and (2.15). The values of $w_{\rm rms}$ and $\theta_{\rm rms}$ have been divided by 277 and 0·205 respectively.

boundary (either the same or different boundaries); sometimes one is concentrated near both boundaries while the other is mainly near one; and sometimes they both are concentrated near both boundaries. In short, all conceivable combinations seem possible. All these variants produce comparable enhancements in the heat flux over the one-mode results. (We have never produced a reduction in N by the addition of high overtone modes.) Finally, when a_2 decreases below 60 the overtones begin to lose their boundary-layer character, and spread through the body of the fluid, achieving the full spread in z when a_2 reaches about 30, which is close to the wavenumber that maximizes N in the one-mode approximation. Regarded as a function of a_2, N attains its maximum of 27·3 at $a_2 = 20$. At this wavenumber the one-mode result is $N = 16{\cdot}2$. Figure 7 illustrates two steady solutions for (F, 13, 14) with $a_1 = 3$. The z-scale is stretched to bring out the structure of the boundary layer.

In the range $30 < a_2 < 50$ we found time-dependent solutions, but the computing time required to decide whether a given case evolves to a periodic solution is too long to permit a thorough survey. Generally, we have observed that most of the solutions of the type discussed in this section have at least two timescales, one associated with the fundamental and one with the overtones. The cases that were run for long times appear to be quasiperiodic. Figure 8 shows the temporal development of a solution for the same parameters as figure 7. This underlines the richness of the solution space: stable steady solutions and time-dependent solutions seem to coexist in parameter space, though we cannot guarantee that the solution of figure 8 does not ultimately become either periodic or even steady.

5. Comparison with experiments

We concentrate on the experiments performed at high Rayleigh numbers, where the flow is time-dependent. Studies with fluids with $\sigma \geqslant 6{\cdot}8$ show that as R is increased above $R_{\rm c}$, after some change in the patterns of steady flow, convection becomes periodic in time (Rossby 1966, 1969; Willis & Deardorff 1967; Krishnamurti 1970). At first only a small fraction of the convection cells partake in the oscillations, but, as R is increased, more join in until almost all the cells in the layer are oscillating

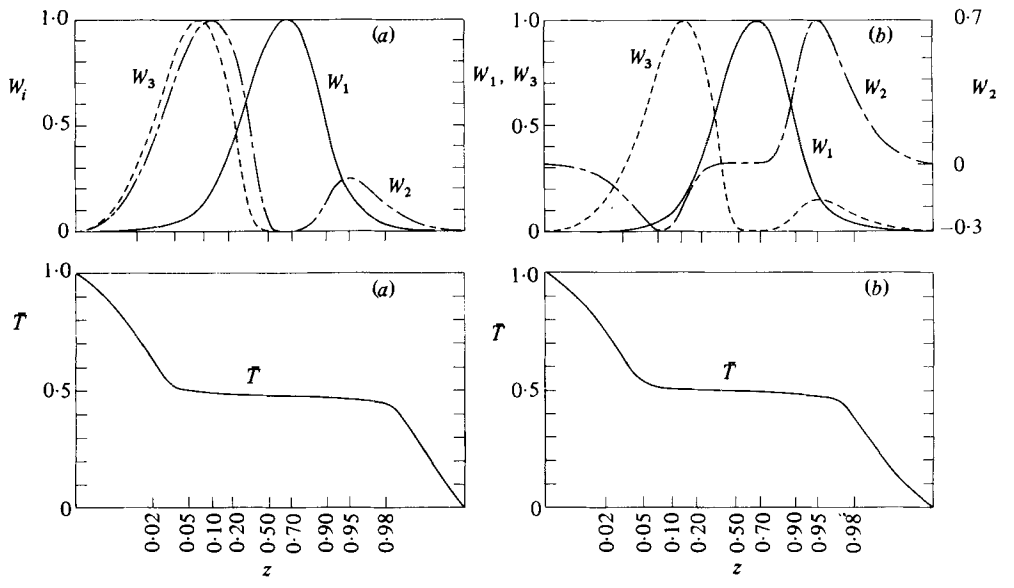

FIGURE 7. Velocity amplitudes and mean temperature of two steady high-overtone solutions for three aligned hexagonal planforms: (F, 13, 14). $R = 10^7$, $\sigma = 10$, $a_i = (3, 39, 42)$. The abscissa is non-uniform in z as indicated. The amplitudes W_i are measured in units of their range $\tilde{W}_i$. (*a*) $\tilde{W}_i = (1042, 283, 194)$, $N = 22{\cdot}4$. (*b*) $\tilde{W}_i = (1045, 61, 318)$, $N = 22{\cdot}0$.

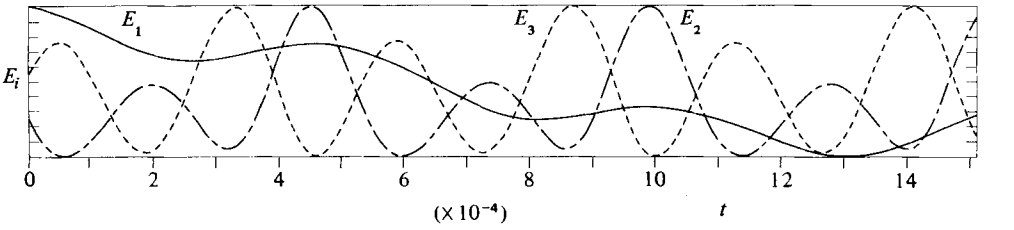

FIGURE 8. Segment of the time variation of the kinetic-energy contributions $E_i(t)$ for a high-overtone solution (F, 13, 14). As in the cases illustrated in figure 7, $R = 10^7$, $\sigma = 10$, $a_i = (3, 39, 42)$. The modes have aligned hexagonal planforms. The fundamental and the overtones each appear to oscillate with their own periods; the ratio of these periods is 4·9. The evolution to this system was slow, and we do not know whether the period ratio has reached a steady value. The kinetic energy E_1 varies between $7{\cdot}42 \times 10^5$ and $7{\cdot}59 \times 10^5$, E_2 between 57·8 and $1{\cdot}43 \times 10^3$, and E_3 between 83·6 and $1{\cdot}10 \times 10^3$.

(Whitehead & Chan 1976; Whitehead & Parsons 1978). This is consistent with the results of Bergé & Dubois (1976), who found intermittent periodic oscillations in velocity at $R = 30R_c$, $\sigma = 130$, though Gollub & Benson (1978) report the onset of strictly periodic oscillations at $R = 20R_c$, $\sigma = 3$. When viewed with a shadowgraph the periodic flows show spoke-shaped patterns, which appear to come and go in time, on a spatial scale somewhat larger than that of the most prominent cells (Busse & Whitehead 1974; J. A. Whitehead 1978 laboratory ciné film of time-dependent convection (private communication)). As R is increased further, the flow becomes aperiodic, though ordered structures are still evident.

At lower Prandtl numbers the situation is somewhat different. The lowest Rayleigh number at which time dependence occurs decreases as σ decreases, and the flow appears to have a higher component of vertical vorticity (see Willis & Deardorff 1970; Rossby 1969; Krishnamurti 1973). Vertical vorticity is also manifest in the steady

flows at lower R (Busse & Clever 1979) and its importance has been discussed in terms of finite-amplitude expansions by Busse (1972) and Clever & Busse (1974). At the lowest Prandtl number at which experiments have been performed (with mercury, $\sigma = 0{\cdot}025$), time dependence sets in for R very close to R_c and is aperiodic at the outset.

The experiments with large-Prandtl-number fluids generally reveal oscillation periods P that decrease with increasing Rayleigh number approximately as $P \propto R^{-\frac{2}{3}}$; often one or more conspicuous overtones (and possibly a subharmonic) of the fundamental period are present. According to Bergé & Dubois (1976) and Gollub & Benson (1978, 1980), who constructed temporal Fourier power spectra of the fluctuating velocities, aperiodicity may first arise simply with the appearance of an overtone whose frequency is incommensurable with that of the fundamental. According to Ahlers & Behringer (1978), who worked with liquid helium in a cylinder with small aspect ratio, the Rayleigh number at which this kind of flow gives way to one with a broad band spectrum decreases as the aspect ratio increases.

There is considerable scatter in the reported periods. Moreover, the transition from steady to oscillatory convection occurs at somewhat different Rayleigh numbers in the various experiments, ranging from 23 to 200 times the critical Rayleigh number R_c. Whitehead & Parsons (1978) tried to reconcile these differences with experimental evidence that convection can choose to be either steady or oscillatory over a considerable range in R, depending on initial conditions. Steady convection can persist to higher R if the initial cellular pattern is forced to be regular, as in the manner of Busse & Whitehead (1974), who artfully induced uniform bimodal planforms. Prominent dislocations introduced into this pattern led to oscillations in portions of the fluid, with the cells developing spoke-like patterns. Although the highest R for which steady bimodal convection can be maintained increases with Prandtl number σ, the Rayleigh number of onset of oscillations in more irregular convection shows no clear variation with σ.

We begin the comparison between our modal solutions and real convection with an examination of the Nusselt numbers. As with the single-mode results, the values of N associated with the two- and three-mode steady solutions vary over a wide range as the wavenumber a_1 is changed. Thus we cannot predict the Nusselt number from these solutions, and in this sense the multimode solutions share the arbitrariness of the single-mode results in II. In principle, if we had a very large number of modes spanning a wide range of wavenumbers, the dominant scales should emerge automatically, but such a calculation is quite impracticable without a substantial decrease in vertical resolution.

A striking feature of the multimode solutions, not exhibited by the single-mode solutions, is the possibility of time dependence. It is clear from table 2 that N is rather insensitive to a_1 in the ranges where periodic solutions are obtained for a given R. Thus for the discussion of the heat flux it does not matter much which of these solutions we choose to compare with the Nusselt numbers of observed time-dependent flows.

The periods of oscillation of our modal solutions do vary with a_1. At fixed R the periods attain a single minimum and appear to become very large as the limits of the wavenumber range of time dependence are approached. Possibly, steady states at these limits are approached by the periods tending to infinity.

For want of an obvious alternative, we have chosen the minimum periods when comparing our results with experiment. In figure 9 we plot these periods for $\sigma = 6{\cdot}8$. The shaded region encompasses the periods observed in the experiments for moderate

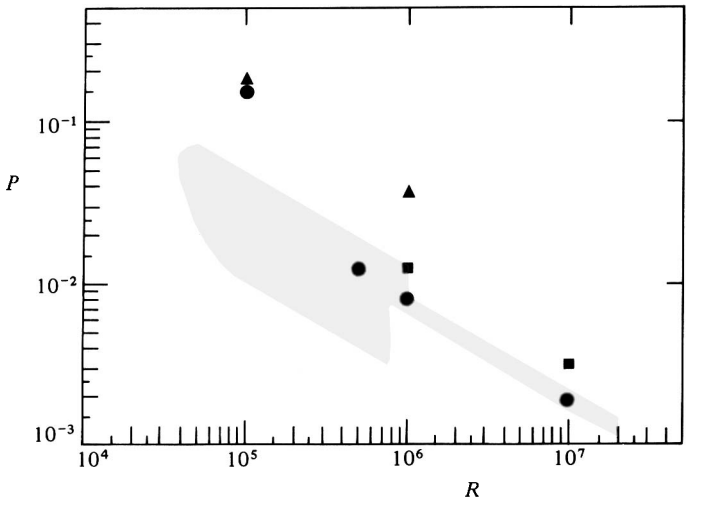

FIGURE 9. Periods of time-dependent numerical solutions compared with those reported from laboratory experiments. The symbols denoting the modal results are as follows: ●, (F, 2); ▲, {F, $\sqrt{3}$}; ■, {F, $\sqrt{3}$, 2}. The shaded area covers the observed periods, which are estimates from Rossby (1969) and Krishnamurti (1973); its narrowness at high R is undoubtedly a result of the paucity of experiments.

σ. Except at $R = 10^5$, the (F, 2) solutions yield periods right on the experimental values, and vary as $R^{-0.62}$, close to the $R^{-\frac{2}{3}}$ variations reported in individual experiments; the three-mode solutions for {F, $\sqrt{3}$, 2} also yield P within the apparent scatter of the laboratory measurements. The narrowness of the shaded band in figure 9 where R exceeds 10^6 simply reflects the paucity of experimental data. The periods obtained with our two-mode solutions at $R = 10^5$ seem to be too high: three-mode solutions there are steady. We cannot offer an explanation of why our results should be worse at low R when we are using a method that one might well expect to deteriorate as R increases. It may well be that, as the low-R edge of the periodic domain is approached, the period goes to infinity, just as (we conjecture) is the case as a_1 approaches the edges of the instability band. However the general variation of P with R is encouraging, suggesting that these simple models may contain some of the physics of the periodic time dependence observed at $R = 10^6$ and 10^7 when the Prandtl number is moderate.

Our main results for the solutions with shortest period are summarized in table 3. The laboratory results are compounded from several sources, since often N was measured only approximately in the studies reporting on the periods P. With our solution choice we obtain a reasonable fit to the measured Nusselt numbers for R between 10^5 and 10^6, though agreement breaks down by 10^7. Moreover, the values of a_1 for which three-mode solutions (in principle, our best representations of convection) are found to be time dependent compare satisfactorily with the wavenumbers below which 90 % of the heat is transported in the experiments of Deardorff & Willis (1967).

We note that the spoke-pattern convection observed at high σ bears some resemblance to the flows obtained with our three-mode periodic solutions. Busse & Whitehead (1974) describe the pattern, which is not unlike what is illustrated in figure 5, but less regular of course. The time dependence apparently takes the form of an oscillation of the spokes, which is sometimes so vigorous that the large-scale visual structure is destroyed temporarily at some epochs in the period. This can be

	1: (F, 2)		2: {F, $\sqrt{3}$}		3: {F, $\sqrt{3}$, 2}		Experiments	
R	N	P	N	P	N	P	N†	P‡
10^5	4·4	0·14	4·1	0·18	—	S	4·5	0·015–0·05
5×10^5	7·7	0·12	—	—	—	S	7·0	0·008–0·02
10^6	10·1	0·0073	7·6	0·038	9·5	0·012	8·5	0·008–0·012
10^7	25·6	0·0018	—	—	25·4	0·0032	16·2	0·002 —

TABLE 3. Comparison of Nusselt numbers N and periods P in typical periodic time-dependent solutions with those reported from laboratory experiments, for $\sigma \simeq 6{\cdot}8$ and several R. S denotes a steady solution and dashes denote an absence of information.

† N values from II, table 1.
‡ P-estimates from Rossby (1969) and Krishnamurti (1973).

seen by looking at individual frames of time-lapse films made by Whitehead in 1978. Thus the periodic appearance and reappearance of large-scale structure (and hence a periodic change in the apparent horizontal scale of the convection) is at least one characteristic of the flow that we reproduce without vertical vorticity. The films also show horizontal distortions of the spokes, which are probably associated with vertical vorticity, though it is not obvious that this is an essential ingredient of the periodic flows.

6. Conclusion

There are several other theoretical treatments of convection that predict time dependence. For example, Lorenz (1963) discovered that time dependence could be found when convection is described with only three normal modes of linear theory. Thus he was led to a model for deterministic chaos. That model may be obtained from our single-mode model (I) by expanding W, Θ, and $\overline{T}$ in Fourier series in z and retaining only one term in each. Yet our single-mode equations never give sustained time dependence, whereas for suitable choice of parameters the Lorenz model does. This difference provides one more illustration of the dangers of drastic truncation, and the lesson applies also to the present work. How should one decide whether the degree of truncation is too severe?

Higher truncations than that of Lorenz have been examined by Saltzman (1962) and Curry (1978) in two dimensions, and by McLaughlin & Martin (1975) in three, and were also found to yield chaotic solutions. The two-dimensional results are disquieting because numerical solutions of the full equations, such as those of Moore & Weiss (1973), are never chaotic, though periodic time dependence sometimes occurs. In a related two-dimensional study by Maschke & Saramito (1979) the number of modes was increased until the results converged in some sense. The criterion used was that the Rayleigh number at the onset of chaos was no longer a function of the number of modes retained. This occurred when about eighty Fourier modes in the horizontal and vertical had been included. It would not be possible to measure the accuracy of our truncation by such standards since effectively we have thousands of vertical modes and just a few horizontal ones. Also, in our procedure, it is not practical to increase the number of horizontal modes by very much. However, the fact that our time dependence resembles some of the flows measured in experiments suggests that, although the three-mode truncation may not serve as an accurate approximation to time-dependent convection, it may provide a useful qualitative model.

Another description of time-dependent buoyant dynamics has been given by Howard (1966). In his picture, a thermal boundary layer forms, thickens to the point of instability, and disrupts to agitate the main body of the fluid, presumably by the motion of thermals. The timescales predicted by Howard agree reasonably well with those measured, and to some extent with our periods. Yet the two qualitative pictures seem different in many ways. However, as we shall explain presently, there are certain similarities, and in any case the two descriptions may well correspond to two diverse physical descriptions of time-dependent convection. In particular, R. Krishnamurti (1980, private communication) has observed recently that time dependence might indeed be caused either by thermals or by the advection of hot spots in cellular motion.

Howard's (1966) model of thermal bursts resulting from convective instability of the boundary layers predicts the period to be the thermal diffusion time across the boundary layers, whereas, if the flow were better described by Welander's (1967) model of hot and cold inhomogeneities advected by the large-scale flow, the turnover time of the fundamental mode is more directly relevant. Actually, as can be seen from the single-mode asymptotic analysis in I, these two times are essentially the same: steady flow occurs when there is a balance between diffusive enlargement of the thermal boundary layers and advective diminution.

Besides these attempts to calculate periods, there have also been fuller discussions of the causes of time dependence. One of the issues that has been raised is the relative importance of buoyancy and inertia in the development of convective oscillations. The Howard model and the Welander tube (Welander 1967; Keller 1966) are controlled by buoyancy; in fact a version of the latter is described by the Lorenz (1963) equations (L. N. Howard & W. V. R. Malkus, unpublished manuscript; Yorke & Yorke 1981). In contrast, in the work of Busse and collaborators the role of the inertial terms is important (Busse 1972; Clever & Busse 1974; Busse & Whitehead 1971, 1974). The analysis by Clever & Busse of the spatially oscillatory instability of bimodal convection, at low Prandtl number and slightly supercritical Rayleigh numbers, seems to reproduce observed periods of time-dependent convection in air reasonably well (Krishnamurti 1970, 1973; Willis & Deardorff 1967, 1970), and agreement with experiments in liquid helium is very good (A. Libchaber 1981 private communication). The instability is a breakdown of purely two-dimensional flow and, at least when $\sigma < 1$, is caused by the excitation of the vertical vorticity modes found in linear theory (Ledoux, Schwarzschild & Spiegel 1961). Our present calculation omits such modes, and therefore cannot reproduce the Busse–Clever transition.

In the case of a hexagon and one or both of its immediate overtones, the overtone modes approximate large-scale inhomogeneities, which are advected by the main mode. In a very rough way the model may be considered analogous to Welander's. In this case the eddy turnover time appears to be important.

The circulation time around a particle flow line is given by

$$\tau = \oint |\mathbf{u}|^{-1} ds, \tag{6.1}$$

where the integral is evaluated around the flow line. This time is determined by two factors: the magnitude of W and the horizontal extent of the eddy. In the single-mode solutions N and W achieve maxima with respect to a at about the same point, but the flow geometry is such that the integral (6.1) increases as a decreases. Thus τ achieves its minimum with respect to a at a value greater than the wavenumber a_m at which N is maximized. On the other hand the boundary-layer thickness ϵ is of order

N^{-1} and achieves its minimum at a_m. Where there are sufficient entries in table 2 to estimate a_m and the wavenumber at which the period is minimized, one can see that the latter exceeds the former, as does the wavenumber at which τ is least.

In an equally crude sense our experiments with boundary-layer dwellers in §4 may be compared with Howard's theory. The growth of the boundary-layer countercells, which eventually destroy and replace their predecessors, proceeds via a conversion of potential energy into kinetic energy, which is subsequently shared with the fundamental mode. The oscillation period of the boundary modes is less than the overturning time of the fundamental mode, and is presumably controlled largely by the boundary-layer instability.

The major part of the numerical studies were carried out in New York at the Goddard Institute for Space Studies of the National Aeronautics and Space Administration. The computer facilities of the National Center for Atmospheric Research in Boulder, sponsored by the National Science Foundation, have been used in further analysis of the time-dependent solutions. This research was supported in part by the National Aeronautics and Space Administration through grants NSG-7511 and NAGW-91, by the Air Force Geophysics Laboratory through contract F19628-77C-0104, and by the National Science Foundation through grants DES74-14439, PHY77-27086 and ATM80-20426. We thank Dr N. O. Weiss for his thoughtful advice.

The Joint Institute for Laboratory Astrophysics is supported jointly by the University of Colorado and the National Bureau of Standards.

Appendix A. Summary of horizontal structure functions

(i) *Two aligned hexagonal planforms* (F, 2). Both planforms are Christopherson hexagons whose functional form is given by

$$f_i(x,y) = \phi(\mathbf{x}, a_i) \equiv (\tfrac{2}{3})^{\frac{1}{2}}[\cos a_i y + 2\cos \tfrac{1}{2}\sqrt{3}\, a_i x \cos \tfrac{1}{2} a_i y].$$

For such hexagons $C_{111} = C_{222} = C \equiv 6^{-\frac{1}{2}}$. When $a_2 = 2a_1$, $C_{112} = \frac{1}{2}C$ and $C_{122} = 0$; otherwise $C_{112} = C_{122} = 0$. The fundamental and the overtone hexagonal planform have the same orientation, and differ in scale by a factor 2. The remaining values of C_{ijk} can be obtained from the symmetry relations $C_{ijk} = C_{jik} = C_{ikj}$.

(ii) *Two rotationally displaced hexagonal planforms* {F, $\sqrt{3}$}. Both planforms are Christopherson hexagons, say $\phi(\mathbf{x}, a_1)$ and $\tilde{\phi}(\mathbf{x}, a_2)$, where $\tilde{\phi}$ is obtained from ϕ by rotating the pattern through an angle α. $C_{111} = C_{222} = C$. $C_{122} = C$ and $C_{122} = 0$ when $a_2 = \sqrt{3}\, a_1$ and α is an integral multiple of $\frac{1}{6}\pi$; otherwise $C_{112} = C_{122} = 0$.

(iii) *Two aligned square planforms* [F, 2]. In this case $f_i = \cos a_i x + \cos a_i y$; $C_{111} = C_{222} = 0$, and, when $a_2 = 2a_1$, $C_{112} = \frac{1}{4}$ and $C_{122} = 0$.

(iv) *A hexagonal planform and its two first overtones* {F, $\sqrt{3}$, 2}. This is a Christopherson hexagon plus its two overtones as described in (i) and (ii): $f_1 = \phi(\mathbf{x}, a_1)$, $f_2 = \tilde{\phi}(\mathbf{x}, a_2)$, $f_3 = \phi(\mathbf{x}, a_3)$, where $a_2 = \sqrt{3}\, a_1$ and $a_3 = 2a_1$. $C_{111} = C_{222} = C_{333} = C_{112} = C_{123} = C$, $C_{113} = \frac{1}{2}C$ and $C_{122} = C_{223} = C_{233} = 0$.

(v) *Three parallel interacting hexagonal planforms* (F, n, $n+1$). This is a combination of three planforms $f_i = \phi(\mathbf{x}, a_i)$ whose wavenumbers are made to satisfy $a_2 = na_1$, $a_3 = (n+1)a_1$ in order that fluctuation interactions be represented. $C_{ijk} = 0$ unless i, j and k are either equal or all different, in which case the value is $\frac{1}{2}C$.

REFERENCES

AHLERS, G. & BEHRINGER, R. P. 1978 Evolution of turbulence from the Rayleigh–Bénard instability. *Phys. Rev. Lett.* **40**, 712–716.

BERGÉ, P. & DUBOIS, M. 1976 Time dependent velocity in Rayleigh–Bénard convection: a transition to turbulence. *Optics Commun.* **19**, 129–133.

BUSSE, F. H. 1969 On Howard's upper bound for heat transport by turbulent convection. *J. Fluid Mech.* **37**, 457–477.

BUSSE, F. H. 1972 The oscillatory instability of convection rolls in a low Prandtl number fluid. *J. Fluid Mech.* **52**, 97–112.

BUSSE, F. H. & CLEVER, R. M. 1979 Instabilities of convection rolls in a fluid of moderate Prandtl number. *J. Fluid Mech.* **91**, 319–335.

BUSSE, F. H. & WHITEHEAD, J. A. 1971 Instabilities of convection rolls in a high Prandtl number fluid. *J. Fluid Mech.* **47**, 305–320.

BUSSE, F. H. & WHITEHEAD, J. A. 1974 Oscillatory and collective instabilities in large Prandtl number convection. *J. Fluid Mech.* **66**, 67–80.

CHAN, S. K. 1971 Infinite Prandtl number turbulent convection. *Stud. Appl. Math.* **50**, 13–49.

CLEVER, R. M. & BUSSE, F. H. 1974 Transition to time-dependent convection. *J. Fluid Mech.* **65**, 625–645.

CURRY, J. H. 1978 A generalized Lorenz system. *Commun. Math. Phys.* **60**, 193–204.

DEARDORFF, J. W. & WILLIS, G. E. 1967 Investigation of turbulent thermal convection between horizontal plates. *J. Fluid Mech.* **28**, 675–704.

GOLLUB, J. P. & BENSON, S. V. 1978 Chaotic response to periodic perturbation of a convecting fluid. *Phys. Rev. Lett.* **41**, 948–951.

GOLLUB, J. P. & BENSON, S. V. 1980 Many routes to turbulent convection. *J. Fluid Mech.* **100**, 449–470.

GOUGH, D. O., SPIEGEL, E. A. & TOOMRE, J. 1975*a* Modal equations for cellular convection. *J. Fluid Mech.* **68**, 695–719 (Paper I).

GOUGH, D. O., SPIEGEL, E. A. & TOOMRE, J. 1975*b* Highly stretched meshes as functionals of solutions. In *Proc. 4th Int. Conf. Numer. Meth. Fluid Mech.* (ed. R. D. Richtmyer). Lecture Notes in Physics, vol. 35, pp. 191–196.

HOWARD, L. N. 1966 Convection at high Rayleigh number. In *Proc. 11th Int. Congr. Appl. Mech.* (ed. H. Görtler), pp. 1109–1115. Springer.

JONES, C. A. & MOORE, D. R. 1979 The stability of axisymmetric convection. *Geophys. Astrophys. Fluid Dyn.* **11**, 245–270.

JONES, C. A., MOORE, D. R. & WEISS, N. O. 1976 Axisymmetric convection in a cylinder. *J. Fluid Mech.* **73**, 353–388.

KELLER, J. B. 1966 Periodic oscillations in a model of thermal convection. *J. Fluid Mech.* **26**, 599–606.

KRISHNAMURTI, R. 1970 On the transition to turbulent convection. Part 2. The transition to time-dependent flow. *J. Fluid Mech.* **42**, 309–320.

KRISHNAMURTI, R. 1973 Some further studies on the transition to turbulent convection. *J. Fluid Mech.* **60**, 285–303.

LEDOUX, P., SCHWARZSCHILD, M. & SPIEGEL, E. A. 1961 On the spectrum of turbulent convection. *Astrophys. J.* **133**, 184–197.

LORENZ, E. N. 1963 Deterministic nonperiodic flow. *J. Atmos. Sci.* **20**, 130–141.

MCLAUGHLIN, J. B & MARTIN, P. C. 1975 Transition to turbulence in a statically stressed fluid system. *Phys. Rev.* A **12**, 186–203.

MASCHKE, E. K. & SARAMITO, B. 1979 On the possible importance of generalized Lorenz equations in the theory of magnetohydrodynamic stability. In *Intrinsic Stochasticity in Plasmas* (ed. G. Laval & D. Gresillon), pp. 383–392. Orsay: Editions de Physique.

MOORE, D. R. & WEISS, N. O. 1973 Two-dimensional Rayleigh–Bénard convection. *J. Fluid Mech.* **58**, 289–312.

ROBERTS, P. H. 1966 On non-linear Bénard convection. In *Non-Equilibrium Thermodynamics, Variational Techniques, and Stability* (ed. R. Donnelly, R. Hermann & I. Prigogine), pp. 125–162. University of Chicago Press.

ROSSBY, H. T. 1966 An experimental study of Bénard convection with and without rotation. Ph.D. thesis, Massachusetts Institute of Technology.

ROSSBY, H. T. 1969 A study of Bénard convection with and without rotation. *J. Fluid Mech.* **36**, 309–335.

SALTZMAN, B. 1962 Finite amplitude free convection as an initial value problem. *J. Atmos. Sci.* **19**, 329–341.

SPIEGEL, E. A. 1971 Convection in stars. I. Basic Boussinesq convection. *Ann. Rev. Astron. Astrophys.* **9**, 323–352.

TOOMRE, J., GOUGH, D. O. & SPIEGEL, E. A. 1977 Numerical solutions of single-mode convection equations. *J. Fluid Mech.* **79**, 1–31 (Paper II).

WELANDER, P. 1967 On the oscillatory instability of a differentially heated fluid loop. *J. Fluid Mech.* **29**, 17–30.

WHITEHEAD, J. A. & CHAN, G. L. 1976 Stability of Rayleigh–Bénard convection rolls and bimodal flow at moderate Prandtl numbers. *Dyn. Atmos. Oceans* **1**, 33–49.

WHITEHEAD, J. A. & PARSONS, B. 1978 Observations of convection at Rayleigh numbers up to 760,000 in a fluid with large Prandtl number. *Geophys. Astrophys. Fluid Dyn.* **9**, 201–217.

WILLIS, G. E. & DEARDORFF, J. W. 1967 Development of short-period temperature fluctuations in thermal convection. *Phys. Fluids* **10**, 931–937.

WILLIS, G. E. & DEARDORFF, J. W. 1970 The oscillatory motions of Rayleigh convection. *J. Fluid Mech.* **44**, 661–672.

YORKE, J. A. & YORKE, E. D. 1981 Chaotic behavior and fluid dynamics. In *Hydrodynamic Instabilities and the Transition to Turbulence* (ed. H. L. Swinney & J. P. Gollub), pp. 77–95. Springer.